Physico-Mechanical Behaviour of Oil Palm Broom Fibres (OPBF) as Eco-friendly Building Material

Emmanuel Owoichoechi MOMOH[1] Adelaja Israel OSOFERO[2*] Alfonso MARTINEZ-FELIPE[3]

Fazlena HAMZAH[4]

School of Engineering, University of Aberdeen, Kings College, Aberdeen, United Kingdom[1,2,3]

Faculty of Chemical Engineering, Universiti Teknologi MARA, UiTM Shah Alam, Selangor, Malaysia[4]

r01eom18@abdn.ac.uk[1], aiosofero@abdn.ac.uk[2], a.martinez-felipe@abdn.ac.uk[3], fazlena@salam.uitm.edu.my[4]

Abstract

Until recently, the rib of the leaflets of the oil palm tree was only used for making brooms due to its stiffness and durability. However, the mechanical properties of this fibre are unknown. Due to the geometrical variation of the cross-section of the fibres along their length, this study divided them into 4-categories. The result of this study reveals that the fibres have a specific gravity between 0.45-0.84 and diameter varying between 0.20 mm (at the tail) and 4.00 mm (at the cap). Maximum tensile strength of 900 MPa was recorded. Scanning electron microscopy of fibre cross-sections revealed graded cavities concentrated at the core but a densely packed cortex. This radial and longitudinal density gradient is responsible for the phenomenon whereby the fibres are stiffer in bending but possess reduced tensile strength towards the cap. Further investigations carried out on the fibres include water absorption, chemical composition and thermogravimetric analysis. The fibre is proposed for use as natural-fibre reinforcement in cement and polymeric composites as it is cheap, and void of high carbon footprints associated with the use of conventional reinforcement materials in construction.

Keywords: Cement composite; Characterisation; Elaeis guineensis; Mechanical properties; Natural Fibre; Oil Palm Broom Fibres; Physical Properties; Sustainable materials.

[*]Corresponding Author: OSOFERO, Adelaja Israel

Email: aiosofero@abdn.ac.uk

Phone: +44 (0)1224 274255

(Authors' surnames are capitalized)

1.0 INTRODUCTION

The oil palm tree is a monocotyledon of the family *Arecaceae* with the scientific name *Elaeis guineensis.* Though of African origin, it thrives on tropical soils and is, therefore, abundant in 3 continents of the world, namely; Africa, Asia and South America and serves as the major source of palm oil [1]. Oil palm is reported to be the highest yielding edible oil crop in the world with a lifespan of between 20-30 years [2]. Oil palm is a huge source of vegetable fibres such that Malaysia and Indonesia which are the largest palm oil producers in the world continually face difficulties in managing the wastes generated from its cultivation and processing activities [3].

Among the wastes generated from oil palm plantation sites are oil palm shell, empty fruit bunch fibre (EFBF), oil palm pressed fruit (or mesocarp) fibre (OPMF), oil palm trunk fibres (OPTF) and oil palm frond fibres (OPFF). These are usually disposed indiscriminately or used by the locals as cooking fuel, both of which are not environmentally friendly [3-5]. As a result, several studies have recommended possible uses of the fibres ranging from paper production [6] to structural applications like natural fibre-reinforcement in concrete [7] and polymer composites [8].

1.1 Oil Palm Broom Fibres (OPBF)

Oil palm broom fibres (OPBF) are the ribs of the leaflets of oil palm trees. Studies on OPBF for engineering applications are very few and recent [9,10]. OPBF is presently mainly used as sweeping brooms in many countries around the world. Compared to other oil palm fibres (such as EFBF, OPMF, OPTF and OPFF), OPBF are larger in size with their average diameter ranging from less than 1mm to 3mm and length between 500 and 1200mm. In other words, the fibres possess the least aspect ratio among all oil palm fibres. Fig 1.1 illustrates the location of OPBF in the oil palm leaflets. By physical examination, OPBF seem to be stiff. They do not absorb water readily and do not rot easily like other natural fibres. Generally, oil palm fibres have good resistance to deterioration due to the presence of silica bodies [11]. Cross-sectional dimension of OPBF vary along its length: being thickest at the connection to the leaflet stalk and thinnest at the free end.

The popular extraction technique for OPBF is with the aid of a machete or knife. The leaflets are first detached from the petioles, then the leaves are peeled-off the ribs; herein referred to as OPBF. The fibres are then tied into broom units only to be sold at local markets [9]. Each broom unit consists of between 150-200 individual fibres. The first attempt at automating the fibre-extraction process is reported in the study of Nwankwojike *et al*. [12]. The study designed, developed and patented a palm frond broom peeling machine to reduce drudgery and fatigue associated with its extraction. The electric-powered version of the machine extracts over 6000 broom fibres per hour with an efficiency of 88.33% while the manually-powered version produces only about 2000 broom fibres per hour with an efficiency of 91.7%.

The main chemical constituents of fibres obtained from oil palm tree include, cellulose, lignin, hemicellulose, holocellulose and ash [13]and studies have shown that the tensile strength of the plant matter is proportional to its cellulose content as it is responsible for the plant structure rigidity [14-16].

The development of several structures such as chairs, baskets, roofs, oil palm fibre-concrete [17], oil palm fibre-reinforced earth-bricks [18], oil palm fibre-reinforced polymeric composites [19], insulation panels [20], paper-based products [21] etc, from other oil palm fibres and recent drives towards environmental sustainability has necessitated investigation into some physical and mechanical properties of OPBF for which research information is non-existent at the moment. The uniqueness of OPBF could create a paradigm for both structural and non-structural use of the palm fibre in reinforcement for composites.

2.0 EXPERIMENTAL PROGRAMME

2.1 Specimen sampling and preparation

Oil palm broom fibres (OPBF) were obtained from “Rice and Spice” Aberdeen UK, in the form of broom units. The procedure for extracting the fibres from the palm trees has been discussed in section 1.1. Blemish-free fibres having average length of 0.8 m were selected by visual inspection and handpicking. Fibres. It was observed that OPBF possess an axial gradation in which the fibres are thickest and thinnest in cross-sectional diameter at the head and tail respectively. For this reason, each

fibre was cut into four (4) specimens, each of 150mm length and grouped under four (4) categories. Category A are fibres 150mm long starting from the petiole joint (head) while category B are fibres 150mm long beginning from the end of category A. Similarly, category C are fibres 150mm long beginning from the end of category B and category D being fibres 150mm long beginning from the end of category C (See Fig 2.1). This leaves out about 200mm cut off length at the tail. In other words, this study focused on an OPBF length of 600 mm measured from the head of the fibres. This approach was employed to better understand possible variations in strength behaviour along the length of the fibre. Cross-sectional areas of a total of 150 specimens were measured. All OPBF used for this study were more than 365 days old after harvesting from the oil palm trees. Other tests carried out include measurement of cross-sectional areas of OPBF, determination of moisture content, water-absorption, specific gravity and tensile strength of the OPBF.

In a bid to further understand the structure/stability of OPBF, proximate analysis was carried out according to ASTM D5142–02a [22], using a TGA/SDTA851^{e} thermobalance, supplied by Mettler Toledo, while ultimate analysis was performed using a ThermoFisher Scientific FlashEA 1112 series analyser, according to ASTM D 5373 – 02 [23]. The TGA/SDTA851^{e} thermobalance was also used for the pyrolysis and combustion experiments after calibration with indium and aluminium at an accuracy of ±0.5K and 1.0 μg. About 20 mg of OPBF were weighed inside an aluminium oxide crucible, and placed in the TGA furnace, using nitrogen and air as carrier gases. Firstly, pyrolysis was carried out under nitrogen atmosphere, by heating from room temperature up to 950^{0}C, at a heating rate of 20^{0}C min^{-1}. Then, the sample was exposed to air, in order to promote combustion, from 950^{0}C to 1200^{0}C, at the same heating rate of 20^{0}C min^{-1}.

2.2 Determination of cross-sectional areas of OPBF

Cross-sectional areas of the fibres were measured with the aid of a digital calliper with a precision of 0.01 mm. Due to the varying shapes of the fibre cross-sections, two diameter measurements were recorded for each cross-section and equivalent cross-sectional areas were determined to assume a circular cross-section. To determine the sufficiency of the sample size for determining standard cross-sections, Eqn (1) of ASTM D2915-17 [24] explained in section 3.1 was used.

2.3 Moisture content test

Moisture content determination was carried out in accordance with the requirement of ASTM D4442-16 [25]. The fibres were cut into lengths of 50 mm and placed in a metallic dish. The specimen was weighed and placed in an oven and set to 103^{0}C for 24 hours. The OPBF was then weighed until a constant mass was achieved. Moisture content was calculated using Eqn 2.1*:*

$$MC\ (\%) = \frac{w - w_d}{w_d} \text{ x } 100 \ldots\ldots\ldots\ldots\ldots\ldots\ldots\ldots 2.1$$

where; w = original mass, and w_d = oven-dry mass. The test was carried out on three batches of specimen and the average moisture content of the OPBF was determined.

2.4 Water absorption test

The fibres were cut into lengths of 50 mm, weighed and placed in a plastic jar. Water was added to the specimen in the jar until the specimen was fully submerged and left to stand undisturbed at room temperature. The fibres floated to the surface of the water at the beginning of the test due to their low specific weight. At specified time intervals, the OPBF were taken out of the water, cleaned with a dry cloth, and weighed. Water absorption was calculated using Eqn 2.2.

$$WA\ (\%) = \frac{w_{wet} - w}{w} \text{ x } 100 \ldots\ldots\ldots\ldots\ldots\ldots\ldots\ldots 2.2$$

where; w_{wet} = wet mass of OPBF, and w = original mass of OPBF. The test was carried out on three batches of specimen for 10, 30, 60, 180, 360, 1440, 2880, 7200, 8640 and 11520 minutes.

2.5 Specific gravity determination

The specific gravity of OPBF was determined according to the requirements of ASTM D854 – 14 [26]. The specimens were cut into lengths of 50 mm with the aid of a knife, so they can be put in a pycnometer. Specific gravity was found to be 0.84 at a moisture content of 9.86%. The low specific gravity makes it superior to steel in terms of strength-to-weight ratio. At a moisture content of less than 1%, the specific gravity of OPBF is 0.45. This, therefore, implies that the specific gravity is a function of the moisture content in the fibre at any instantaneous time.

2.6 Tensile strength test

A major indicator of the structural performance of a material is its strength in tension. Tests were performed to measure the tensile strength of OPBF. To avoid damage from the jaw grips of the machine, epoxy glue was applied to the ends of the specimen in the form of a bulb (about 20mm and 4mm in length and thickness respectively) and allowed to set for about 60 hours to allow for sufficient hardening of the glue bulbs prior to testing. This resulted in a specimen gauge length of 110mm (Figs 2.2a and 2.2b). The determination of the tensile strength of the fibres was carried out on a Hounsfield universal testing machine (Model H10KS). Each fibre was inserted into the grips at the bulb ends and secured in a vertical position (see Fig 2.2c). The test was performed according to the requirements of ASTM D4761-13 [27] using a load cell of 3kN in displacement control at 5mm/mm. Average test time for each fibre was 2 minutes. Results from fibres which failed prematurely by pulling-out at the hardened glue ends were discarded. The stress-strain relationships are based on the lowest cross-sectional area of each fibre since the fibres failed at this point (see Fig 2.2d). All off-cut fibres beyond 600mm were neglected from the tensile test. The machine was equipped with a computer and was used to set up load and strain rate and displayed the load-extension curve during testing as well. The measured cross-sectional area and gauge length of each OPBF tested in tension was used to convert the load-deformation curve into the corresponding stress-strain curve. A total of 120 OPBF specimens (that is, 30 specimens for each group) were prepared and tested in tension. Specimens that generated extreme results were neglected and a stress-strain curve was obtained for each category of fibre.

2.7 Microscopic examination of OPBF

Scanning Electron Microscopy (SEM) images of OPBF surfaces and cross-sections were obtained using a CarlZeiss GeminiSEM 300VP scanning electron microscope. A 20nm-thick carbon coating was applied over the OPBF surfaces after which a 10nm-thick sputter coating of gold/palladium alloy (60% Au and 40% Pd) was applied over the carbon coating in order to enhance the conductivity of the samples. SEM was carried out to investigate and understand the shapes of fibre cross-section, fibre morphology and the nature of the failure surfaces. SEM was performed at the Aberdeen Centre for Electron Microscopy, Analysis and Characterisation (ACEMAC), University of Aberdeen, UK.

3.0 RESULT AND DISCUSSION

3.1 Cross-sectional area of OPBF

Mean cross-sectional area of OPBF was calculated as $1.837 mm^2$ with standard deviation s as $0.546\ mm^2$. Substituting appropriate values into Eqn 3.1 gave an n value of 138 specimens for a 95% confidence level. Hence the number of samples investigated (150) for determination of standard cross-sectional areas is sufficient.

$$n = \left(\frac{ts}{\alpha x}\right)^2 \quad \ldots 3.1$$

where n = *sample size*

s = *standard deviation of the specimen values*

x = *specimen mean value*

α = *estimate of precision, (0.05), and*

t = *value of t statistic from Table 1 of* ASTM D2915-17 [24].

The relationship between cross-sectional area and length of OPBF was found to be exponential (Fig 3.1) and can be expressed as Eqn 3.2.

$$A(x) = A_o e^{-\beta x} \quad \ldots 3.2$$

where A is OPBF cross-sectional area (mm^2) at any length x(mm) from the head of the fibre. A_0 is the intercept on the vertical axis of the graph of cross-sectional area *vs* length of OPBF and is equal to *3.7006* for OPBF used in this study (see Fig 3.1). β is the coefficient of x in Eqn 3.2 and is equal to *0.004* for this study. The relationship in Eqn 3.2 could be used as a generic expression for defining the dimension of natural fibres and plant parts in their undamaged condition. It is noteworthy that the performance of a composite is a function of the bond strength between the fibres and the matrix. A variation of cross-sectional area with length also implies a possible variation of bond strength with length. Therefore, Eqn 3.2 presents a quick method for assessing variation in bond strength along the fibres. Furthermore, it is possible to accurately simulate bond stress with respect to the length of fibre if the parameters of Eqn 3.2 are defined. A numerical analysis of the bond pull-out behaviour of OPBF

from a matrix can also be enhanced since the axial pull-out force will depend on the part of the fibre (i.e. head or tail) embedded in the matrix.

3.2 Morphology of OPBF

OPBF possess a rough surface with globular protrusions on the surface of the fibres (Fig 3.2a). This is consistent with the studies of Sreekala *et al.* [28] and Izani *et al.* [29] for EFBF. These protrusions otherwise known as *tyloses* have been reported to improve the bond between EFBF and matrix resin during composite fabrication due to an enhancement in mechanical interlock [28]. The presence of impurities on the surface of the fibres implies that they need to be cleaned in order to enhance bonding with a host matrix. An observation of the cross-section of OPBF (Fig 3.2b) reveals that the filaments making up each fibre are bonded by lignin of varying thickness. This together with unevenly distributed phloem and xylem cavities are responsible for varying inter-filament bond strength. Phloem and xylem are tubules through which water and solutes travel throughout plant members [30]. Under tension, the weakest bonds fail first and the stress is transferred unto another section of the fibre in a sudden manner. This results in brittle shear failure mode experienced at fracture for most of Category-A as can be observed in some of the fractured OPBF (Fig 2.2d).

Among the four categories of fibres tested, D-fibres recorded the highest tensile strengths while A-fibres recorded the lowest tensile strengths. Close observation of the SEM images of the cross-sections of the fibres (Fig 3.2b) reveals that the A-fibres have cross-sectional areas in the range of 2-3.5mm^2 and have filaments around their cortex densely packed, while the core is dominated with cavities in the range of 100-140,000μm^2 in cross-sectional area. As one proceeds down the length of the fibre, the cross-section area reduces with cavities ranging between 1500-7000 μm^2 (see Table 3.1). Therefore, whereas, fibres with larger cross-sections are expected to have higher tensile strength, the effective area of cross-section resisting axial tension is relatively lower than that of the fibres with smaller cross-sections.

Further observation of the longitudinal section showed increasing sideway openings of phloem and xylem tubules towards the cap (head) of the fibres (Fig 3.2c). This creates a truss system which is

biologically engineered and causes the fibre to bear increased bending moments caused by the weight of the leaflets and the action of wind incident upon the leaflets. This is possible through a cell-based mechanosensor which transforms environmental stimulus into a biologically recognisable signal controlling growth characteristic [31]. Consequently, an increase in fibre stiffness towards the stalk (head) of the leaf occurs. Oil palm broom fibres can, therefore, be classified as Natural Functionally Graded Materials (NFGM) and the radial and longitudinal density gradient is responsible for the phenomenon whereby the fibres are stiffer in bending (but possess lesser strength in tension) towards the head. This explains the lower strength values observed for the fibre categories with larger cross-sections.

Due to these cavities, failure in tension is in a sudden brittle manner. This can also be seen from the stress-strain curves. The uneven distribution of cavities causes stress to be borne in an uneven manner across fibre cross-section thereby causing an abrupt change in the effective cross-sectional area resisting tensile stress at a time. Generally, OPBF specimens failed at the point of smallest cross-section just before the epoxy grip end.

3.3 Moisture content of OPBF

Moisture content of OPBF were determined as 9.86%. Puspasari *et al.* [32] recommended that OPFF be dried to a moisture content below *10%* to prevent fungal attack during storage. Usually, the alkalinity of cementitious matrices, will not allow for the growth of fungal organisms. Nonetheless, OPBF because of their size, possess cavities that could trap moisture that will eventually be lost thereby causing shrinkage with subsequent debonding of fibres from the host matrix. Drying the fibres to a moisture content below 10% would minimise dimensional instability and enhance fibre-matrix bond.

3.4 Water absorption behaviour of OPBF

The 24 hours average water absorption of discrete OPBF were determined as 44.7%. This maximum amount of water absorption occurs by capillary action through porous fibre membrane and exposed cavities from the broken ends of the fibres. Danso [33], reported a 54% water absorption for oil palm empty fruit bunch fibres (EFBF) at 24 hours. The study compared the water absorption rates for coconut

fibres, sugarcane bagasse and EFBF. Zawawi *et al* [34] reported more than 80% water absorption for EFBF. Generally, oil palm fibres have a low water absorption capacity compared to other natural fibres. Furthermore, the result obtained in this study indicate that OPBF have the least absorption capacity among oil palm fibres. Some studies have shown that natural fibres usually can absorb more than twice their weight, when exposed to water, in less than 24 hours [33,35].

Fig 3.3 presents water absorption behaviour of unbroken (whole) OPBF and 50mm discrete OPBF in water at room temperature. Water absorption rate for both samples is identical and rapid only in the first 3 hours. OPBF absorbs between 15-20% of its weight within the first 60 minutes after which the rate of absorption slows down. After 11520 minutes (8days), the percentage water absorption was obtained for both samples. Eqn 3.3a and 3.3b were also derived to predict OPBF rate of water absorption at room temperature for discrete OPBF and unbroken OPBF respectively.

$$\%WA = 8.862 \ln(T) - 11.106, \quad \text{3.3a}$$

$$\%WA = 6.4904 \ln(T) - 5.0797, \quad \text{3.3b}$$

where, percentage water absorption *(%WA)* is a function of time *(T)* in minutes. Sreekala *et al.* [36] opines that the main factors that affect oil palm fibres interaction with water are diffusion, permeability of fibre surface and sorption. The increased absorption of the discrete (broken) OPBF is a consequence of exposed cavities at the fibre ends resulting from breakage into discrete units. The delayed absorption between 24 and 48 hours is more pronounced for unbroken OPBF due to sealing of micropores on the surface of the fibres. After soaking the OPBF in water for about 24 hours, the colour of the water changed to brownish-red signifying the dissolution of water-soluble amorphous lignin, waxes and impurities. As a result, the micropores of the fibre surface were exposed and a jump in water absorption is observed for both samples at 48 hours (2880 minutes). This is sometimes referred to as a *two-step* water absorption for natural fibres [36].

Natural fibres due to their organic origin are hydrophilic in nature due to their organic origin. This characteristic threatens their potential to be used as structural materials since their environmental stability could be compromised by moisture. It is therefore important therefore to assess the water

absorption characteristic of OPBF and seek for possible treatments towards enhancing hydrophobicity, or otherwise make recommendations for alternative applications. It also enhances understanding of fibre volume changes with the (un)availability of moisture. In fibre-reinforced concrete, for example, the strength of the composite is enhanced by the bond strength between the fibres and the matrix. The integrity of this bond depends on the degree of dimensional stability of the fibres which is usually governed by fibre water absorption characteristics. In order words, in the presence of water, the increase in fibre volume due to water absorption creates internal stresses in the matrix. This creates cracks that weaken fibre-matrix bond. Conversely, the fibres may lose water under dry condition and shrink. Shrinkage causes the fibres to be de-bonded from the matrix, thereby causing a reduction in fibre-matrix bond strength and subsequent poor performance of the composite.

3.5 Tensile strength of OPBF

Observation of the stress-strain curves reveal that OPBF failure is not pre-empted by any warning and the fibres fail in a sudden brittle manner. Fig 3.4 presents the stress-strain relationships of the 4 categories of fibres. The stress-strain curves of OPBF (Fig 3.4) shows an initial non-linear part at the onset of loading. Bourmaud *et al.* [37] refers to this phenomenon as *fibrillar reorientation* and attributes it to the reorientation of cellulose fibres due to shear action within the polysaccharide chain during loading. In other words, at the onset of loading, the microfibrils making up natural fibres begin to stretch and increase in length. Beyond a certain limit, the stretch stops and the load is borne in a linear elastic manner until fracture. The linear zone is as a result of cellulose fibrils becoming aligned in the axis of tensile loading. It is believed that the tensile strength of natural fibre is proportional to its cellulose content [14,28,38].

Table 3.1: Summary of Tensile Properties of OPBF

OPBF Group	Average cross-sectional Area (mm^2)	Average Largest Single Cavity in cross-section (μm^2)	Average Max. Tensile strength (MPa)	Average Maximum Strain (mm/mm)
A	3.659 ± 0.916	137,500	300.54	0.0534 ± 0.0105
B	1.893 ± 0.569	48,760	312.35	0.0464 ± 0.0103
C	1.107 ± 0.373	21,150	389.86	0.0463 ± 0.0087
D	0.688 ± 0.324	7,420	555.28	0.0383 ± 0.0090
Average	1.837 ± 0.546	NA	389.51	0.0461 ± 0.0128

The relationship between tensile strength and cross-sectional area of OPBF shown in Fig 3.5, corroborates the findings of Genet *et al.* [14]. Although the correlation is poor, it is not unusual. Natural fibres show high variability in both mechanical and physical properties even if derived from the same plant [39]. Some factors responsible for such variability are the presence of natural defects located within the fibre tissues during growth and development of the parent plant and build-up of plant tissue within strategic areas to withstand forces of nature (e.g. wind) during plant life [31].

There is also a correlation between the strain at failure e and the cross-sectional area at the point of fracture of OPBF sample and it is expressed as Eqn 3.4. Fig 3.6 shows the relationship between strain at failure and cross-sectional area of OPBF.

$$e = 0.0081\, ln\, A + 0.0427 \quad \ldots\ldots 3.4$$

Where e is the maximum OPBF strain (mm/mm) and A is the cross-sectional area (mm^2) at the point of fracture of OPBF sample.

Overall, category-D OPBF have the highest tensile strength while the tensile strength seems to reduce with increase in cross-sectional area. Hence, category-A OPBF recorded the lowest tensile strength. This is true for cellulosic fibres [14]. The axial and longitudinal gradation of cavities is responsible for such behaviour and this is revealed in the SEM images (Fig 3.2a, b and c) obtained and discussed in section 3.2.

3.6 Proximate and thermogravimetric analysis

Fig 3.7 shows the weight loss (TG) and derivative thermogravimetric (DTG) curves, obtained by proximate analysis of 20 mg of Oil Palm Broom Fibres (OPBF), including pyrolysis (T < 950°C) and combustion (T > 950°C). Pyrolytic thermal degradation can be divided into three stages: moisture desorption (below 150°C), main devolatilisation, and continuous slight devolatilization [40]. The proximate analysis indicates that OPBF consist of 6.5% moisture, 53.8% volatile carbon matter, 28% ash and 11.53% fixed carbon.

The volatile carbon matter (53.8 %) was released in the main devolatilization step, which ranges from 170^{o}C to 530^{o}C, through two main processes ($T_{p,1}$ = 306°C and $T_{p,2}$ = 361°C) [41,42]. Thermal decomposition of the fibres takes place through a complex mechanism that is greatly influenced by heat and mass transfer [43]. The appearance of different peaks in the DTG curve of Fig 3.7, suggests that the different fractions of the fibres maintain their identities and their decomposition is in distinguishable steps [41].

The relative intensities of the peaks in Fig 3.7 can be then related to the amounts of hemicelluloses, cellulose and lignin present in the sample. More precisely, the main degradation process, $T_{p,2}$ = 361°C, is associated to the thermal decomposition of cellulose, while decomposition of hemicellulose takes place at slightly lower temperatures, $T_{p,1}$ = 306°C [44]. Lignin, on the other hand, is expected to decompose at lower rates, and over a wider range of temperature (137 – 667°C) [41], due to the presence of various oxygen functional groups. Their cleavage releases low molecular weight products, while the complete rearrangement of the backbone at higher temperatures leads to the formation of char and to the release of volatile products [45]. As a result, lignin degradation may be obscured by the other prominent thermal degradation processes shown in Fig 3.7, and only the low-intensity shoulder

observed between 400°C and 550°C is visible, corresponding to the latest states of lignin devolatisation and char oxidation [40,44].

Overall, these results are in excellent agreement with average compositions of cellulose, hemicellulose and lignin reported for other biomass, in the 40 - 45%, 30 - 35 % and 20 - 25 % (weight %) ranges, respectively [46-48] and indicate a limited interaction between these components in the fibres. The maximum decomposition rate for the combustion of the OPBF takes place at 970°C and is associated with the formation of ash at high temperature. The element composition of the OPBF was determined using ultimate analysis, resulting in C = 52.5 %, N = 9.8 %, H = 1.8% and O = 35.9% (weight %). This result is also consistent with the composition of the fibre in terms of cellulose, hemicellulose and lignin, derived from the TG and DTG curves.

A comparison of the thermogravimetric data for OPBF and oil palm empty fruit bunch fibres (EFBF) presented in other studies [28,29,49,50] show that OPBF has better resistance to thermal degradation. Findings from this thermogravimetric analysis will help to develop design guidance and recommendations for OPBF-reinforced elements' fire-resistance. In addition, the findings will be useful for further studies aimed at determining appropriate treatment techniques for enhancing physical, thermal and mechanical properties of OPBF.

3.7 Use of OPBF in composites

Like other natural fibres, there may be durability concerns associated with the use of OPBF as reinforcement for composites. Concerns include the presence of impurities that are non-compatible with the host matrix, presence of hemicellulose, lignin and oils which easily decompose at the fibre-matrix interface, moisture-prone dimensional instability [13,28,29] and alkali-induced embrittlement of fibres (in cementitious matrix) [7,9]. However, treatment methods such as alkalisation, silanization, acetylation [28] and hot water treatment [29] have been reported to eliminate fibre impurities, modify fibre surfaces, enhance fibre hydrophobicity and improve tensile strength. Consequently, durability can be enhanced, and the overall performance of the composites improved through these treatments [34,38]. A study of an appropriate treatment method for OPBF is recommended. Nevertheless, untreated OPBF

have been successfully employed as reinforcement for laterite-based roofing tiles [10] with 100% increase in flexural strength of the roofing tiles due to the addition of OPBF mesh.

Due to the range of tensile strength (200-900 MPa) and size of OPBF, it is possible to develop reinforcement tendons by combining more than one OPBF. The fibres can be twisted together in a helical form and held together as tendon units by hose clamps. The use of hose clamps on bamboo reinforcement bars was reported to improve bamboo-concrete bond with the clamps acting as shear connectors [51]. Likewise, OPBF tendons can be used as reinforcement bars in cementitious matrices to increase mechanical (shear) interlock between fibres and matrix. A study in this direction is therefore recommended.

4.0 THEORETICAL PREDICTIONS

4.1 Empirical equations

According to Sreekala *et al.* [28], the major predictors of tensile strength (σ) properties for a natural fibre are its fibrillar structure, micro-fibrillar angle and cellulose content (w). Using the correlation between strain *e*, and micro-fibrillar angle α as stated in Eqn 4.1 and 4.2, and using the corresponding average values from Table 3.1, we have the following;

$$e = 0.0077\alpha^2 + 0.0728\alpha + 2.78 \quad \text{.....4.1}$$

$$\sigma = 12.22w - 2.830\alpha - 334.005 \quad \text{.....4.2}$$

The micro-fibrillar angle of OPBF is found to be 15^0 and the cellulose content of OPBF by weight is calculated as *62.3%* from Eqn 4.2. Bourmaud *et al*. [37] reported that natural fibres with low microfibrillar angle are characterized by higher tensile strength. On the other hand, the calculated cellulose content falls within the range reported in the review of Momoh and Osofero [9] for other oil palm fibres but is not within the range deduced from section 3.6 of this study. This implies that the prediction equations (Eqns 4.1 and 4.2) alone may not be adequate for OPBF. Generally, high cellulose content and low micro-fibrillar angle is believed to make OPBF stiffest among oil palm fibres. A more direct method of measuring cellulose content in OPBF is advised.

4.2 Finite element modelling of OPBF in tension

Tensile behaviour of OPBF can also be predicted by linear finite element procedure. Fig 3.4 suggests that the behaviour of OPBF between onset of loading till failure can be approximated to be elastic. Therefore, in modelling for tension, an OPBF strand can be modelled as a one-dimensional bar element considering its low aspect ratio. Now consider an OPBF with length L (Fig. 4.1) fixed at one end (A) and free at the other (B) with internal stresses b due to an externally applied tension T. Then the mathematical expression is of the form given by Koutramanos [52]:

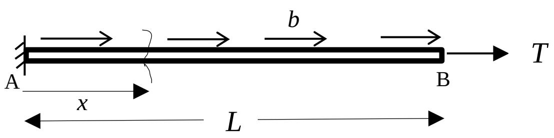

Fig 4.1: One-dimensional illustration of OPBF

$$\frac{dT}{dx} + b(x) = 0 \quad \ldots 4.3$$

In this case, however, the axial force T can be re-written in terms of axial strain thus;

$$E\frac{\partial^2 u}{\partial x^2} + b(x) = 0 \quad \ldots 4.4$$

To approximate the solution over the entire OPBF domain, the weak form of Eqn 4.4 is found by multiplying both sides by an arbitrary virtual displacement δu and integrating over the whole length of the fibre so that;

$$\int_0^L \delta u \left(E\frac{\partial^2 u}{\partial x^2} + b \right) dx = 0 \quad \ldots 4.5$$

Integrating Eqn 4.5 by parts gives;

$$-\int_0^L \frac{\partial \delta u}{\partial x}.E.\frac{\partial u}{\partial x} dx + \int_0^l \delta u b dx + \left(\delta u.E.\frac{\partial u}{\partial x} \right) = 0 \quad \ldots 4.6$$

Then using the general expression for strain can be written as;

$$u(x) \approx \sum \emptyset_i . u_i \equiv N.d \quad \ldots 4.7$$

then; $\delta u(x) \approx N.\delta d$ and hence, $N.\delta d = \delta d^T . N^T$

where $\emptyset_i . u_i$ is the elemental linear shape function and *N* is the sum of all elemental shape functions. Furthermore, *δu(x)* can be substituted with $\delta d^T . N^T$ in Eqn 4.6 to give the form of Eqn 4.8.

$$-\int_0^L \frac{\partial(\delta d^T . N^T)}{\partial x} . E . \frac{\partial(N . d)}{\partial x} dx + \int_0^l \delta d^T . N . b . dx + (\delta d^T . N^T . \sigma) = 0 \quad \ldots\ldots 4.8$$

Re-arranging Eqn 4.8;

$$\delta d^T \left(\int_0^L \frac{\partial N^T}{\partial x} . E . \frac{\partial N}{\partial x} dx . d \right) = \delta d^T \left(\int_0^L N^T . b dx + (N^T \sigma) \right) \quad \ldots\ldots 4.9$$

Or simply;

$$\delta d^T (k . d - f) = 0 \quad \ldots\ldots 4.10$$

Where;

$$k = \int_0^L \frac{\partial N^T}{\partial x} . E . \frac{\partial N}{\partial x} dx \; and \; f = \int_0^L N^T . b dx + (N^T \sigma) \quad \ldots\ldots 4.11$$

This holds true if;

$$\boldsymbol{k.d = f} \quad \ldots\ldots 4.12$$

which is, in fact, Hooke's law of elasticity.

Therefore, for every element of OPBF in pure axial tension, the elemental stiffnesses k_i can be integrated for each finite element (e_i) and then summed up to be solved in the form of algebraic equations. Therefore;

$$k_i = \begin{pmatrix} \frac{\partial \emptyset_i}{\partial x} \\ \frac{\partial \emptyset_{i+1}}{\partial x} \end{pmatrix} . E . \begin{pmatrix} \frac{\partial \emptyset_i}{\partial x} & \frac{\partial \emptyset_{i+1}}{\partial x} \end{pmatrix} \quad \ldots\ldots 4.13$$

and

$$f = \sum \int_0^h \begin{pmatrix} \emptyset_i \\ \emptyset_{i+1} \end{pmatrix} b dx \quad \ldots\ldots 4.14$$

where $\emptyset_i$ is the elemental shape function at node *i*, *h* is the length of each finite OPBF element and *k* is stiffness as a function of OPBF elastic modulus and dimensions. Future direction for this research would

be to apply this fundamental derivation to the simulation of fibre behaviour in a commercially available finite element software such as ABAQUS.

5.0 CONCLUSIONS

The following conclusions can be made from this study:

- OPBF possess good tensile strength. Average tensile strength of OPBF at 400 days after harvesting is 389 MPa,
- There exist radial and longitudinal density gradient along the length of OPBF which promotes stiffening on bending (but reduces tensile strength) towards the cap,
- The relationship between cross-sectional diameter and length of OPBF can be expressed by the following generic expression:

$$A(x) = A_0 \, e^{-\beta x}$$

  where A is the OPBF cross-sectional area (mm^2) at any length x (mm) from the head of the fibre, $A_0 = 3.7006$ is the intercept of the curve of cross-sectional area vs length, and $\beta = 0.004$ is the coefficient of x,
- Also, the relationship between strain at failure and cross-sectional area at the point of failure of OPBF sample can be expressed with the following mathematical expression:

$$e = 0.0081 \ln A + 0.0427$$

  where e is the maximum OPBF strain (mm/mm) and A is the cross-sectional area at the point of fracture,
- Thermal degradation of OPBF becomes rapid at a temperature of 361^{o}C,
- A theoretical estimation of the cellulose content in OPBF is given as 62.3% (by weight),
- Appropriate OPBF pre-treatment is recommended to improve quality.

OPBF is cheap and can be obtained at a minimal/no cost in developing countries. Due to its availability, affordability, lightweight, non-toxicity, environmental friendliness, size and good tensile properties, OPBF can be employed as a reinforcement in concrete and polymer composites either as discrete fibres or as tendons analogous to steel reinforcement fibres/bars.

Recommendation

All investigations in this study were carried out at an OPBF-moisture content of 9.8% and at a fibre age of about 400 days. The effect of moisture content and age on the physical and mechanical properties of OPBF would enhance understanding of its behaviour and inform decisions on possible applications in both polymeric and cement composites.

Acknowledgement

Funding for this work was provided by the Petroleum Technology Development Fund (PTDF) of Nigeria.

References

[1] D Mazlan and ASM Abdul Awal (2012) Properties of cement based composites containing oil palm stem as fiber reinforcement, Malaysian Journal of Civil Engineering 107-117.

[2] E Barcelos, Sd-A Rios, RNV Cunha, R Lopez, SY Motoike, E Babiychuk, A Skirycz and S Kushnir (2015) Oil palm natural diversity and the potential for yield improvement, Frontiers in Plant Science, 190(6):1-16.

[3] MA Mannan and C Ganapathy (2004) Concrete from an agricultural waste-oil palm shell (OPS), Building and Environment, 39(4):441-448.

[4] R Dungani, M Jawaid, HPS Abdul Khalil, J Jasni, S Aprilia, KR Hakeem, S Hartati and MN Islam (2013) A review on quality enhancement of oil palm trunk waste by resin impregnation: future materials, Bioresources, 8(2):3136-3156.

[5] F Owolabi, AW Taiwo, AFM Alkarkhi and A Ghazali (2017) optimization of the strength properties of waste, Journal of Natural Fibers, 14(4):551-563.

[6] WR Wan Daud and K-N Law (2011) Oil palm fibers as papermaking material: potentials and challenges, Bioresources, 6(1):901-917.

[7] PSA Lertwattanaruk (2015) Properties of natural fiber cement materials containing coconut coir and oil palm fibers for residential building applications, Construction and Building Materials, 94(1):664-669.

[8] MS Sreekala, J George, MG Kumaran and S Thomas (2002) The mechanical performance of hybrid phenol-formaldehyde-based composites reinforced with glass and oil palm fibres, Composites science and technology, 62(3):339-353.

[9] EO Momoh and AI Osofero (2019) Recent developments in the application of oil palm fibres in cement composites, Frontiers of Structural and Civil Engineering, *in press*.

[10] EO Momoh and BI Dahunsi (2017) Suitability of oil-palm-broom-fibres as reinforcement for laterite-based roof tiles, International Journal of Software & Hardware Research in Engineering, 5(4):27-35.

[11] FN Omar, MAP Mohammed and AS Baharuddin (2014) Effect of silica bodies on the mechanical behaviour of oil palm empty fruit bunch fibres, BioResources, 9(4): 7041-7058.

[12] BN Nwankwojike, JC Agunwamba and OS Onwuka (2014) Design and development of palm frond broom peeling machine, Patent No: NG/P/2014/117, Nigeria.

[13] HPS Abdul Khalil, M Jawaid, MT Hassan and AZ Paridah (2012) Oil palm biomass fibres and recent advancement in oil palm biomass fibres based hybrid biocomposites, *In* Composites and their applications, United Kingdom, IntechOpen, 2012, pp. 187-220.

[14] M Genet, A Stokes, F Salin, SB Mickovski, T Fourcaud, J-F.Dumail and RV Beek (2005) The influence of cellulose content on tensile strength in tree roots, Plant and Soil, 278(1):1-9.

[15] G Norayr, DH Page and MG Paice (1992) The effect of cellulose degradation on the strength of wood pulp fibres, Nordic Pulp and Paper Research Journal, 7(3):152-154.

[16] D Jones, GO Ormondroyd, SF Curling, C-M Popescu and M-C Popescu (2017) Chemical compositions of natural fibres, *In* Advanced high strength natural fibre composites in construction, Woodhead Publishing, pp. 23-58.

[17] P Shafigh, MZ Jumaat, HB Mahmud and NAA Hamid (2012) Lightweight concrete made from crushed oil palm shell: Tensile strength and effect of initial curing on compressive strength, Construction and Building Materials, 27:252-258.

[18] M Noorsaidi (2010) Comparison study on oil palm trunk and oil palm fruit bunch fibre, Modern Applied Science, 4(7):119-129.

[19] MS Sreekala, J George, MG Kumaran and S Thomas (2002) The mechanical performance of hybrid phenol-formaldehyde-based composites reinforced with glass and oil palm fibres, Composites Science and Technology, 62(3):339-353, 2002.

[20] CC Ferrández-Garcia, CE Ferrández-Garcia, M Ferrández-Villena, MT Ferrández-Garcia and T García-Ortuno (2017) Acoustic and thermal evaluation of palm panels as building material, Bioresources, 12(4):8047-8057.

[21] ASM Kassim, AA Mohd, I Nadiah, ZM Hafeez and ZNFA Dayang (2006) Oil palm leaf fibre and its suitability for paper-based products, ARPN Journal of Engineering and Applied Sciences, 11(11):7364-7369.

525 [22] ASTM D5142-02a (2002) Standard test methods for proximate analysis of the analysis
526 sample of coal and coke by instrumental procedures. ASTM International, West
527 Conshohocken, PA.
528 [23] ASTM D5373-02 (2002) Standard test methods for instrumental determination of carbon,
529 hydrogen, and nitrogen in laboratory samples of coal and coke, ASTM International, West
530 Conshohocken, PA.
531 [24] ASTM D2915–17 (2017) standard practice for sampling and data-analysis for structural wood
532 and wood-based products, ASTM International, West Conshohocken, PA.
533 [25] ASTM D4442-16 (2016) Standard test methods for direct moisture content measurement of
534 wood and wood-based materials, ASTM International, West Conshohocken, PA.
535 [26] ASTM D854-14, Standard Test Methods for Specific Gravity of Soil Solids by Water
536 Pycnometer, ASTM International, West Conshohocken, PA.
537 [27] ASTM D4761-13 (2013) Standard test methods for mechanical properties of lumber and
538 wood-base structural material. ASTM International, West Conshohocken, PA.
539 [28] MS Sreekala, MG Kumaran and T Sabu (1997) Oil Palm Fibers: morphology, chemical
540 composition, surface modification, and mechanical properties, Journal of Applied Polymer
541 Science, 66(5):821-835.
542 [29] MN Izani, MT Paridah, UMK Anwar, MM Nor and PS H'ng (2013) Effects of fiber treatment
543 on morphology, tensile and gravimetric analysis of oil palm empty fruit bunches fibers,
544 Composites Part B: Engineering, 45(1):1251-1257.
545 [30] JR Dinenny and MF Yanofsky (2004) Vascular patterning: Xylem or Phloem? Current
546 Biology 14(3): 112-114.
547 [31] F Nogata and H Takahashi (1995) Intelligent functionally graded material: Bamboo,
548 Composites Engineering, 5(7):743-751.
549 [32] I Puspasari, MZM Talib, WRW Daud and SM Tasirin (2014) Characteristic drying curve of
550 oil palm fibers, International Journal on Advanced Science, Engineering and Information
551 Technology, 4(1):20-24.

552 [33] H Danso (2017) Properties of coconut, oil palm and bagasse fibres: as potential building
553 materials, *In* 3rd International Conference on Natural Fibers: Advanced materials for a
554 greener world, ICNF 2017, 21-23 June 2017, Braga, Portugal, Procedia Engineering.
555 [34] I Zawawi, M Ahmad, AA Astimar, R Ramli, MA Jamaludin, M Suhaimi and HA Aisyah
556 (2016) Dimensional stability properties of medium density fibreboard (mdf) from treated oil
557 palm (Elaeis guineensis) empty fruit bunches (EFB) fibres, Chemistry and Materials Science,
558 6:99-99.
559 [35] VS Sharma, BM Marwaha and HK Vinayak (2016) Enhancing durability of adobe by natural
560 reinforcement for propagating sustainable mud housing, International Journal of Sustainable
561 Built Environment, 5:141-155.
562 [36] MS Sreekala, J George, MG Kumaran and S Thomas (2001) Water-sorption kinetics in oil
563 palm fibers, Journal of Polymer Science Part B: Polymer Physics, 39(11):1215-1223.
564 [37] A Bourmaud, C Morvan, A Bouali and V Placet (2012) Relationship between micro-fibrillar
565 angle, mechanical properties and biochemical composition of flax fibers, Industrial Crops and
566 Products, 44:343-351.
567 [38] DSR Petroudy (2017) Physical and mechanical properties of natural fibers, *In* Advanced high
568 strength natural fibre composites in construction, Elsevier, pp. 59-83.
569 [39] S Mukhopadhyay, R Fangueiro and V Shivankar (2009) Variability of tensile properties of
570 fibers from pseudostem of banana plant, Textile Research Journal, 79(5):387-393.
571 [40] M Carrier, A Loppinet-Serani, D Denux, J-M Lasnier, F Ham-Pichavant, C Aymonier and C
572 Francois (2011) Thermogravimetric analysis as a new method to determine the lignocellulosic
573 composition of biomass, Biomass and Bioenergy, 35(1):298-307.
574 [41] D Vamvuka, E Kakaras, E Kastanaki and P Grammelis (2003) Pyrolysis characteristics and
575 kinetics of biomass residuals mixtures with lignite, Fuel, 82(15-17):1949-1960.
576 [42] K Ismail, Z Zakaria and MAM Ishak (2005) Thermal behaviour study of mukah balingian
577 coal and biomass blends during pyrolysis via thermogravimetric analysis, *In* 22nd Annual
578 International Pittsburgh Coal Conference, Pittsburgh.

[43] JA Caballero, JA Conesa, R Font and A Marcilla (1997) Pyrolysis kinetics of almond shells and olive stones considering their organic fractions, Journal of Analytical and Applied Pyrolysis, 42(2):159-175.

[44] A Dhahak, R Bounaceur, C Le-Dreff-Lorimier, G Schmidt, G Trouve and F Battin-Lecler (2019) Development of a detailed kinetic model for the combustion of biomass, Fuel, 242:756-774.

[45] NT Farrokh, H Suopajarvi, P Sulasami and T Fabritius (2018) A thermogravimetric analysis of lignin char combustion, Energy Procedia, 158:1241-1248.

[46] F Hamzah, A Idris and TK Shuan (2011) Preliminary study on enzymatic hydrolysis of treated oil palm (Elaeis) empty fruit bunches fibre (EFB) by using combination of cellulase beta 1-4 glucosidase, Biomass and Bioenergy, 35(3):1055-1059.

[47] M Brebu and C Vasile (2010) Thermal degradation of lignin - a review, Cellulose Chemistry and Technology, 44(9):353-363.

[48] MA Amezcua-Allieri and J Aburto (2018) Conversion of lignin to heat and power, chemicals or fuels into the transmission energy strategy, *In* Lignin - Trends and Applications, Intech Open, pp. 145-160.

[49] SS Idris, N Abd Rahman, K Ismail, AB Alias, Z Abd Rashid and MJ Aris (2010) Investigation on thermochemical behaviour of low rank Malaysian coal oil palm biomass and their blends during pyrolysis via thermogravimetric analysis (TGA), Bioresource Technology, 101:4584-4592.

[50] S Kormin, AZM Rus and SMM Azahari (2017) Thermal properties of biopolyol from oil palm fruit fibre (OPFF) using solvolysis liquefaction technique, *In* IOP Conference Series: Materials Science and Engineering, 244:1-6.

[51] M Muhtar, S Dewi, U Wisnumurti and A Munawir (2019) Enhancing bamboo reinforcement using a hose-clamp to increase bond-stress and slip resistance, Journal of Building Engineering 26**:** 100896.

[52] I Koutromanos (2018) Fundamentals of finite element analysis: linear finite element analysis, Wiley, London, United Kingdom.

Physico-Mechanical Behaviour of Oil Palm Broom Fibres as Eco-friendly Building Material

Emmanuel Owoichoechi MOMOH[1] Adelaja Israel OSOFERO[2] Alfonso MARTINEZ-FELIPE[3]
Fazlena HAMZAH[4]
School of Engineering, University of Aberdeen, Kings College, Aberdeen, United Kingdom[1,2,3]
Faculty of Chemical Engineering, Universiti Teknologi MARA (UiTM) Shah Alam, Selangor, Malaysia[4]
Email: r01eom18@abdn.ac.uk[1], aiosofero@abdn.ac.uk[2], a.martinez-felipe@abdn.ac.uk[3], fazlena@salam.uitm.edu.my[4]

FIGURES

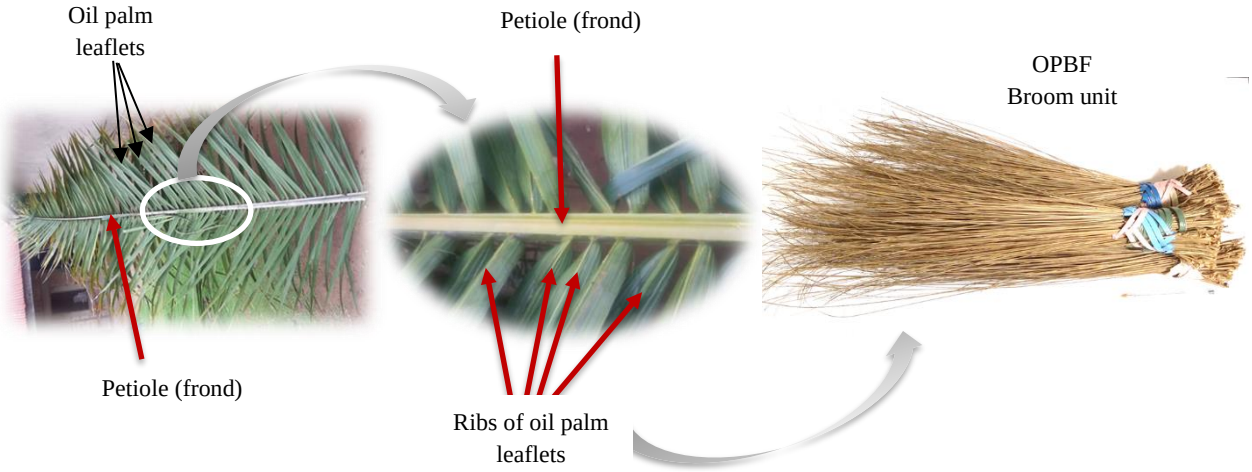

Fig 1.1: Illustration of OPBF from Oil palm fronds

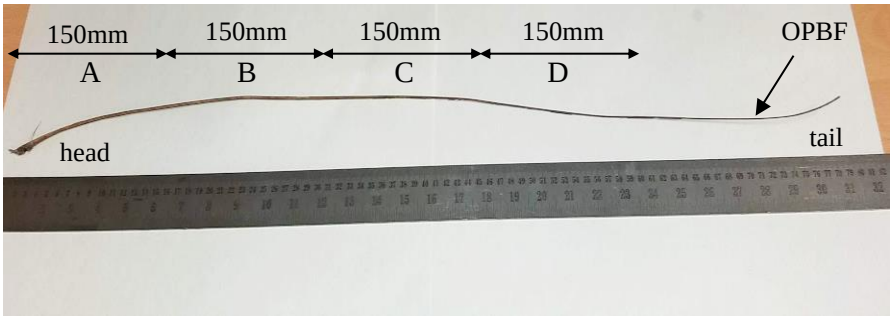

Fig 2.1: Illustration of the 4-Categories of OPBF

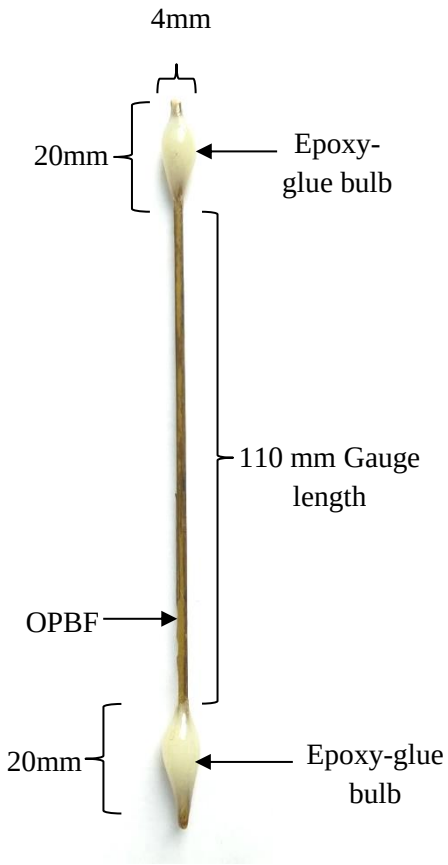

Fig. 2.2a: An OPBF prepared for tensile test

Fig 2.2b: Some OPBF prepared for Tensile Testing

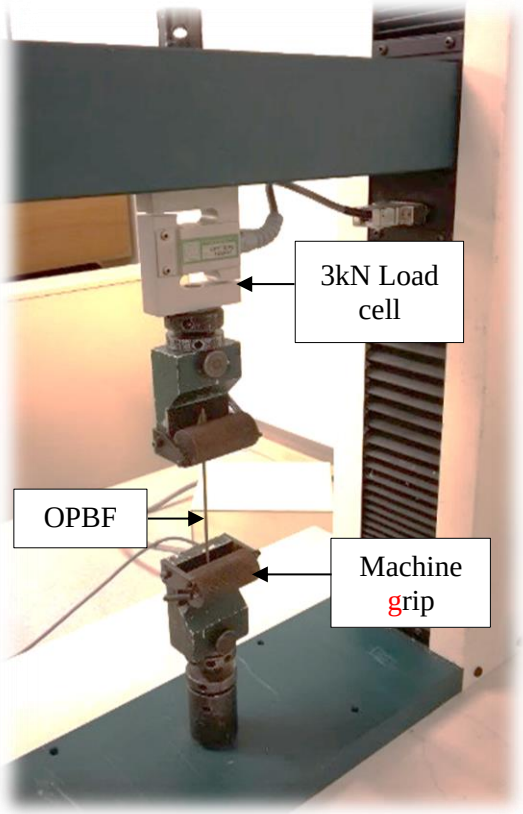

Fig 2.2c: An OPBF sample mounted on machine grips for Tensile Testing

635

Fig 2.2d: Some OPBF samples tested in tension to failure (Tensile-shear failure mode for Category-A fibres)

636

637

638

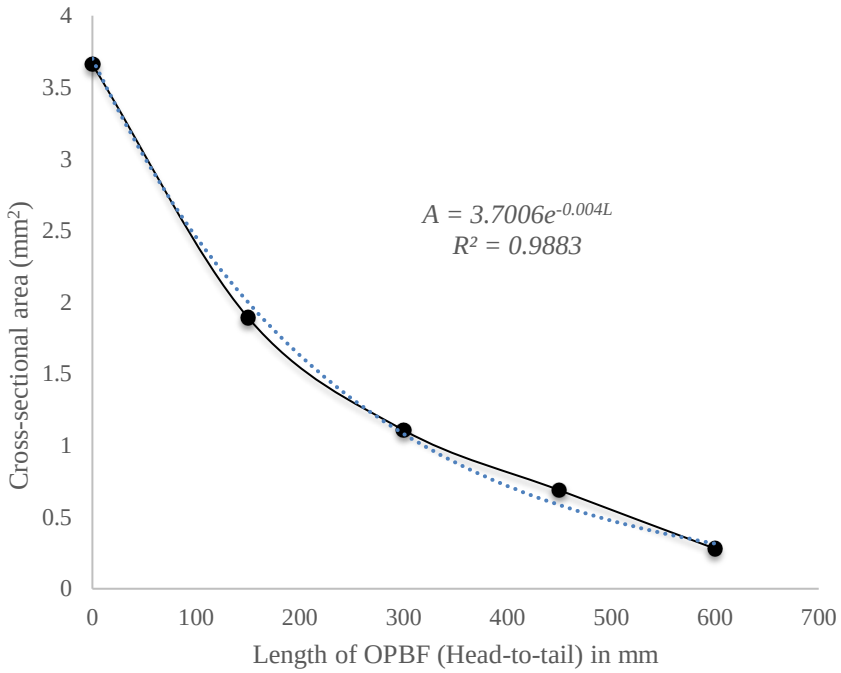

Fig 3.1 Relationship between OPBF cross-sectional area and length

639

640

641

642

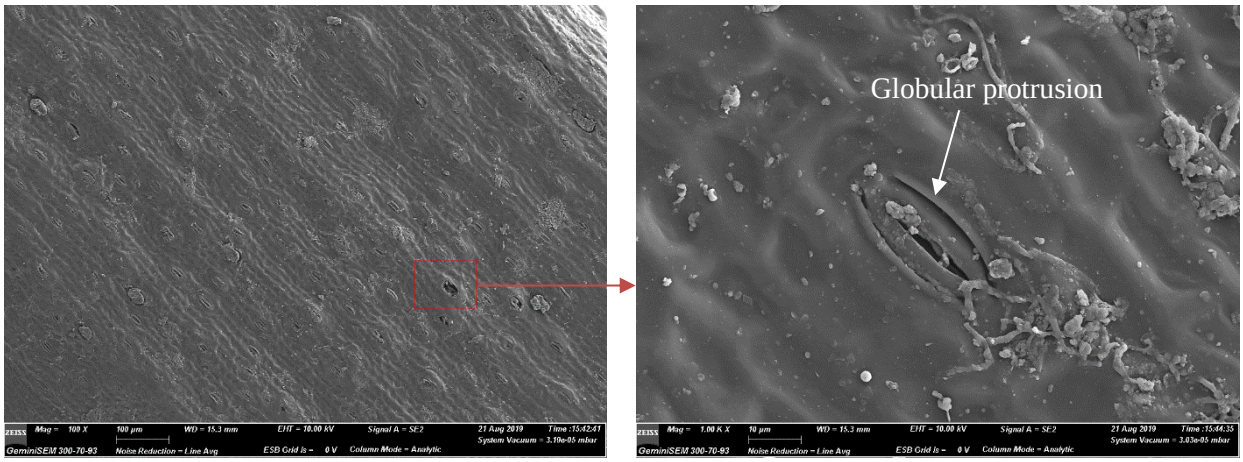

Fig 3.2a: SEM images of OPBF surface: 100X (left): 1000X (right)

643

644

645

646

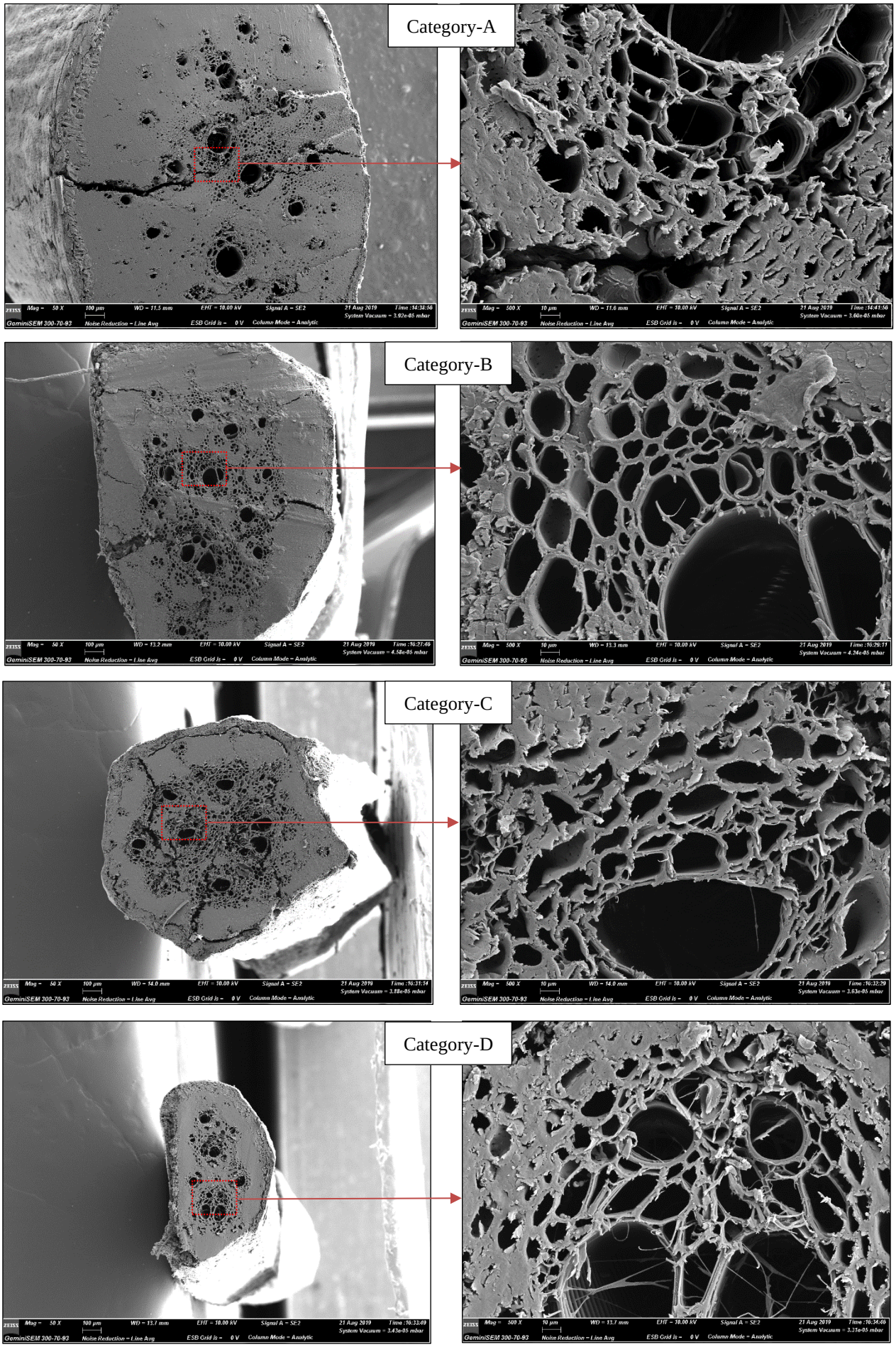

Fig 3.2b: SEM images of OPBF cross-sections: 50X (left): 500X (right)

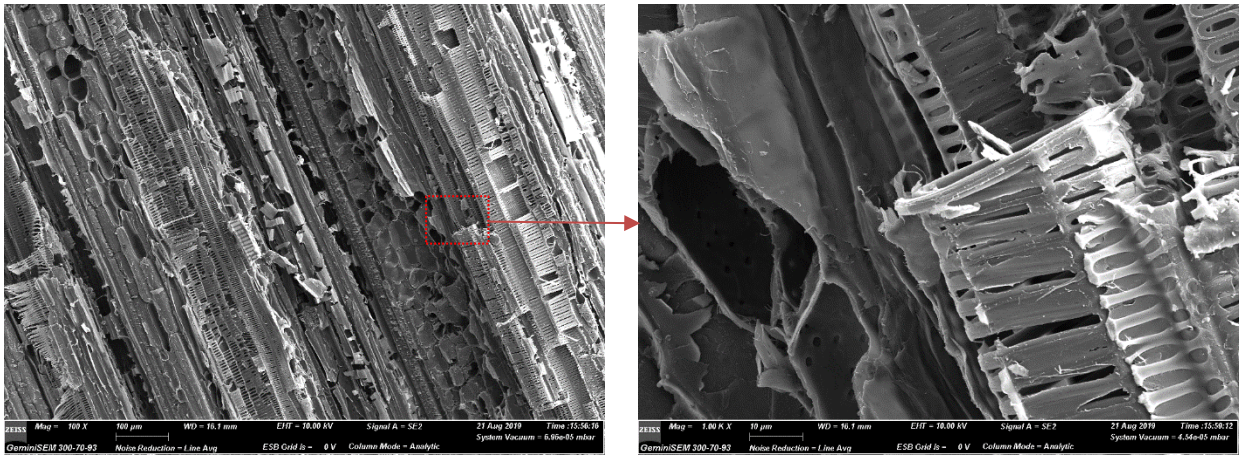

Fig 3.2c: SEM images of OPBF longitudinal section: 50X (left): 1000X (right)

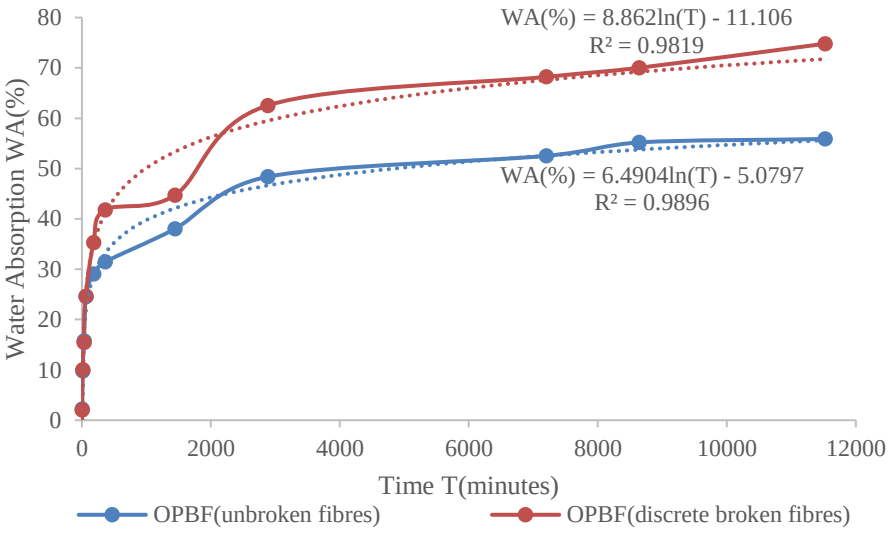

Fig 3.3: Water absorption behaviour of OPBF

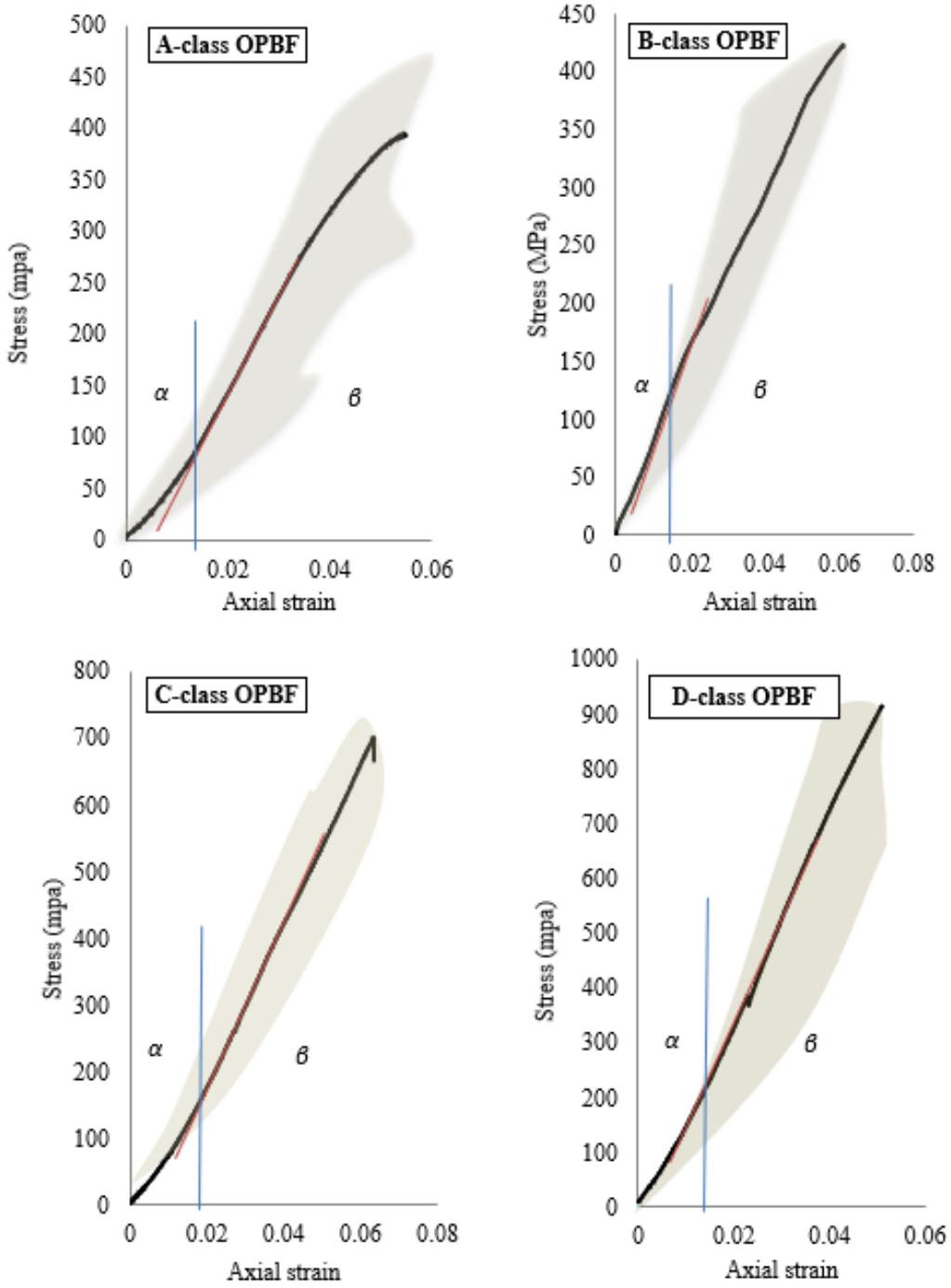

α = region of fibrillar re-orientation
β = region after fibrillar re-orientation

Fig 3.4: Stress-strain envelops of the four categories of OPBF

676

677

678

679

680

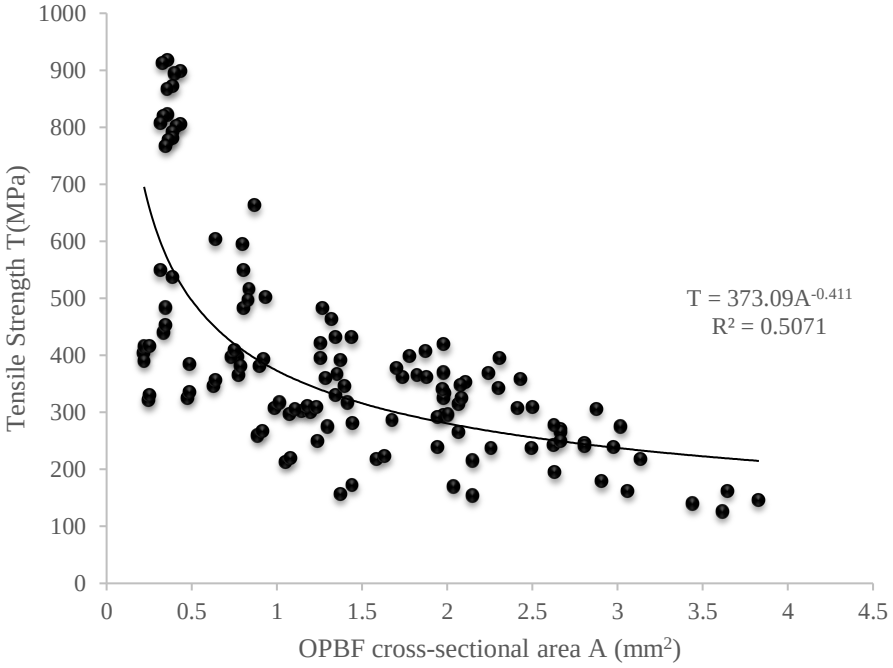

Fig 3.5: Correlation between cross-sectional area and tensile strength of OPBF

681

682

683

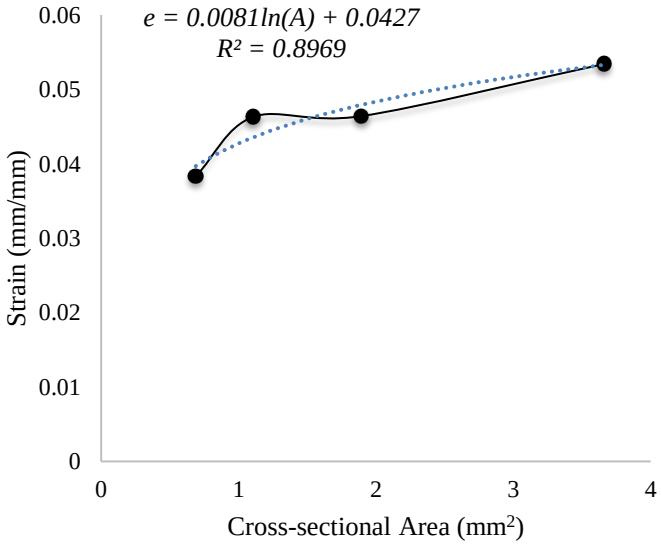

Fig 3.6 Relationship between strain at failure and cross-sectional area of OPBF

684

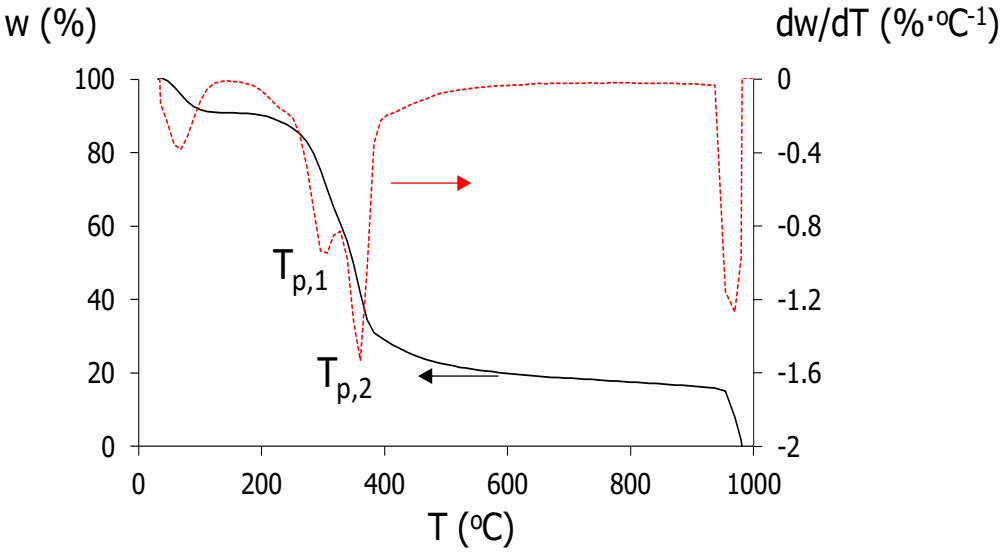

Fig 3.7: Thermogravimetric (TG) and derivative thermogravimetric (DTG) curves corresponding to the pyrolysis (T < 950°C) and combustion (T > 950°C) of Oil Palm Broom Fibres (OPBF).

Physico-Mechanical Behaviour of Oil Palm Broom Fibres as Eco-friendly Building Material

Emmanuel Owoichoechi Momoh[1] Adelaja Israel Osofero[2] Alfonso Martinez-felipe[3]
Fazlena Hamzah[4]
School of Engineering, University of Aberdeen, Kings College, Aberdeen, United Kingdom[1,2,3]
Faculty of Chemical Engineering, Universiti Teknologi MARA (UiTM) Shah Alam, Selangor, Malaysia[4]
Email: r01eom18@abdn.ac.uk[1], aiosofero@abdn.ac.uk[2], a.martinez-felipe@abdn.ac.uk[3], fazlena@salam.uitm.edu.my[4]

LIST OF FIGURES